THE ARCHIVE OF MECHANICAL ENGINEERING

VOL. LVIII 2011 Number 4

10.2478/v10180-011-0023-5

Key words: multibody dynamics, vibrations, stability, feedback control, industrial problems

ACHIM FISCHER[*], *PETER EBERHARD* [*]

SIMULATION-BASED STABILITY ANALYSIS OF A THIN-WALLED CYLINDER DURING TURNING WITH IMPROVEMENTS USING AN ADAPTRONIC TURNING CHISEL

The dynamics of the turning process of a thin-walled cylinder in manufacturing is modeled using flexible multibody system theory. The obtained model is time varying due to workpiece rotation and tool feed and retarded, due to repeated cutting of the same surface. Instabilites can occur due to these consecutive cuts that must be avoided in practical application because of the detrimental effects on workpiece, tool and possibly the machine. Neglecting the small feed, the stability of the resulting periodic system with time-delay can be analyzed using the semi-discretization method.

The use of an adaptronic tool holder comprising actuators and sensors to improve the dynamic stability is then investigated. Different control concepts, two collocated and two model-based, are implemented in simulation and tuned to increase the domain of stable cutting. Cutting of a moderately thin workpiece exhibits instabilities mainly due to tool vibration. In this case, the stability boundary can be significantly improved. When the instability is due to workpiece vibration, the collocated concepts fail completely. Model based concepts can still obtain some improvements, but are sensitive to modeling errors in the coupling of workpiece and tool.

1. Introduction

In machining technology, the striving for even higher machining speeds at good surface finish is limited by the occurrence of vibrations of workpiece and tool. These vibrations, called chatter, are inherently self-excited and do not only lead to a poor surface quality, but also cause tool wear and can even damage tool, workpiece and machine. In [1], four chatter mechanisms have been identified. Of those, regenerative chatter, which is caused by con-

[*] *Institute of Engineering and Computational Mechanics, University of Stuttgart, Pfaffenwaldring 9, 70569 Stuttgart, Germany;*
E-mail: [achim.fischer,peter.eberhard]@itm.uni-stuttgart.de

secutive cuts on the same surface, is the most important by occurrence and intensity. In general, it is modeled as an interaction between the dynamics of the machine structure and the time-delay of the system. The resulting dynamics is described by a set of delay-differential equations (DDE). Because of the detrimental effects on the machining operation, the dynamic stability of the process needs to be analyzed and unstable machining must be avoided. Stability depends not only on the dynamical properties of the system, but also on the process parameters like rotational velocity and depth or width of cut. It is usually characterized in terms of those parameters and displayed in so called stability charts.

In this contribution, stability of the inside turning operation of thin-walled cylinders is investigated and then improved using modern control theory. First, a model of the process is derived using flexible multibody system theory, [2], which can account for the large, nonlinear described rotations of the cylinder as well as the small elastic deformations of cylinder and tool.

Then, a stability analysis of the resulting system is performed using an approximation as a discrete system via the Semi-Discretization Method, [3]. To improve the dynamic behavior a feedback control, based on the adaptronic turning chisel shown in Figure 2, is conceived. Several control laws, ranging from simple collocated concepts to advanced model based methods, are implemented and compared. The different methods are rated by their influence on the stability domain.

2. System Model

Figure 1 shows a schematic view of the considered system. Workpiece and tool are elastic bodies coupled by the process force $\boldsymbol{F}_p$. In addition to the small elastic deformations caused by this process force, the workpiece performs large nonlinear rotations around its symmetry axis with rotational velocity ω. The tool is fixed to the machine structure and moves with the feed velocity v_f toward the jaw.

2.1. Adaptronic tool holder

Figure 2 shows an exploded view of the adaptronic tool. It consists of a turning chisel typically used for inside turning clamped into a tool holder. The top of the tool holder is rigidly attached to the turret of the lathe. The holder was designed to accomodate a piezo stack actuator and contains the drillings necessary for cooling and power supply. The piezo is restrained between two disc shaped endpieces. An eddy current sensor is placed next

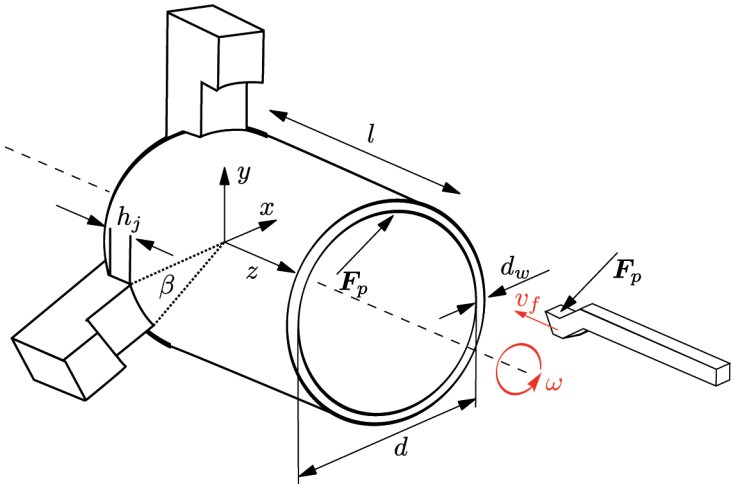

Fig. 1. Workpiece and tool coupled by cutting force law

to the actuator and allows to precisely capture the elongations of the stack. When an external voltage is applied to the piezo stack, a force is generated that acts as a pressure on the two disc shaped pieces clamping the actuator. An additional accelerometer can be placed next to the tool tip and allows to better capture the tip vibrations.

The blade that is used to cut the material is made of hardened high-speed steel and fixed to the chisel. It can be considered as rigid.

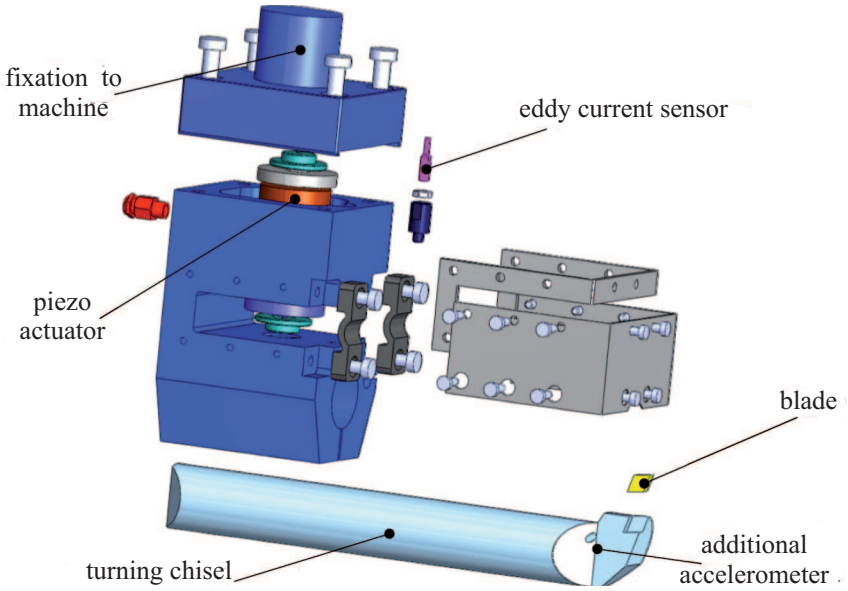

Fig. 2. Active tool comprising actuators and sensors

The Finite-Element-Method (FEM) is used to derive a model of the tool in terms of nodal displacements $\boldsymbol{x}_{f,t}$. For this, the commercial software *Ansys* is used. First, the tool geometry is built and subsequently meshed using the implemented 'solid45' 8-node continuum element. The piezo actuator is modeled as a force element in parallel to a spring whose stiffness is set equal to the stiffness of the stack, $k_{piezo} = 6 \cdot 10^8$N/mm. The resulting equations of motion read

$$\boldsymbol{M}_{f,t} \cdot \ddot{\boldsymbol{x}}_{f,t} + \boldsymbol{D}_{f,t} \cdot \dot{\boldsymbol{x}}_{f,t} + \boldsymbol{K}_{f,t} \cdot \boldsymbol{x}_{f,t} = \boldsymbol{f}_{e,t} = \begin{bmatrix} \boldsymbol{B}_{p,t} & \boldsymbol{B}_{u,t} \end{bmatrix} \cdot \begin{bmatrix} \boldsymbol{F}_p(t) \\ u(t) \end{bmatrix}. \tag{1}$$

The flexible mass-, stiffness and damping matrices $\boldsymbol{M}_{f,t} \in \mathbb{R}^{N_t \times N_t}$, $\boldsymbol{D}_{f,t} \in \mathbb{R}^{N_t \times N_t}$ and $\boldsymbol{K}_{f,t} \in \mathbb{R}^{N_t \times N_t}$ obtained from Finite-Element-Analysis (FEA) describe the dynamic behaviour of the tool under the influence of the external forces $\boldsymbol{f}_{e,t}$. The input matrix $[\boldsymbol{B}_{p,t} \quad \boldsymbol{B}_{u,t}]$ projects hereby the acting forces on the nodal degrees of freedom (dofs). Acting forces are the process force $\boldsymbol{F}_p(t)$ and the force $u(t)$ generated by the piezo stack. The latter will serve as the control input for the feedback design. To reduce the number N_t of nodal dofs needed as inputs, interface nodes are added that serve as application points for $\boldsymbol{F}_p(t)$ and $u(t)$. Figure 3a shows the interface for the piezo actuator force, Figure 3b the interface node for the process force. Those nodes are kinematically bound to the contact surfaces of actuator and cutter. The lighter lines represent those kinematic bindings. Note that part of the model has been made transparent.

The displacement at the tool center point (TCP), $\boldsymbol{y}_{p,t}$, needed for the calculation of $\boldsymbol{F}_p$, and the available measurements for the controller design, $\boldsymbol{y}_{m,t}$, are grouped into the output vector $\boldsymbol{y}_t$,

$$\boldsymbol{y}_t = \begin{bmatrix} \boldsymbol{y}_{p,t} \\ \boldsymbol{y}_{m,t} \end{bmatrix} = \begin{bmatrix} \boldsymbol{C}_{p,t} \\ \boldsymbol{C}_{m,t} \end{bmatrix} \cdot \boldsymbol{x}_{f,t}. \tag{2}$$

Because the rigid body motion of the tool is very small, no additional terms are needed to account for it. For the considered application, feed velocities v_f are typically in the range of a few mm/s.

2.2. Workpiece

The workpiece is a hollow steel cylinder of length l, inner diameter d and wall thickness d_w, as shown in Figure 1. The cylinder is clamped into a three jaw chuck of height h_j. Each of the jaws covers an angle β of the circumference. Flexible Multibody System Theory, [2], will be used to account for the small elastic deformations of the workpiece as well as

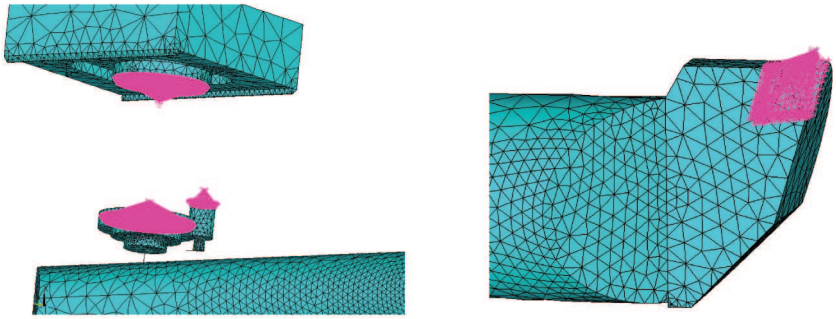

(a) Piezo-actuator input and eddy current sensor output

(b) At the TCP for cutting force input and accelerometer output

Fig. 3. Interface nodes and constraints for tool in- and outputs

the large nonlinear described rotations. The general movement of a flexible body consists of deformations caused by internal or external forces and large displacements and rotations, the rigid body motion. If the deformations of the workpiece remain small, i.e. linear describable and elastic, as it is true in the considered case, its equation of motion can be written in the form,

$$\begin{bmatrix} \boldsymbol{M}_{rr,wp} & \boldsymbol{M}_{rf,wp} \\ \boldsymbol{M}_{fr,wp} & \boldsymbol{M}_{ff,wp} \end{bmatrix} \cdot \begin{bmatrix} \ddot{\boldsymbol{x}}_{r,wp} \\ \ddot{\boldsymbol{x}}_{f,wp} \end{bmatrix} = \begin{bmatrix} \boldsymbol{h}_{r,wp} \\ \boldsymbol{h}_{f,wp} \end{bmatrix} + \begin{bmatrix} \boldsymbol{0} \\ -\boldsymbol{K}_{f,wp} \cdot \boldsymbol{x}_{f,wp} - \boldsymbol{D}_{f,wp} \cdot \dot{\boldsymbol{x}}_{f,wp} \end{bmatrix} + \begin{bmatrix} \boldsymbol{0} \\ \boldsymbol{f}_{e,wp} \end{bmatrix}. \tag{3}$$

The rigid body motion is hereby described by the displacements and rotations of a body fixed reference frame grouped in $\boldsymbol{x}_{r,wp} \in \mathbb{R}^6$. The frame of reference of the cylinder is fixed to the jaws and located on the symmetry-axis as shown in Figure 1. Using the FEM, the deformations are described by a number of nodal displacements $\boldsymbol{x}_{f,wp} \in \mathbb{R}^{N_{wp}}$ given with respect to the body fixed frame. The submatrices $\boldsymbol{M}_{ff,wp}$, $\boldsymbol{D}_{f,wp}$, $\boldsymbol{K}_{f,wp} \in \mathbb{R}^{N_{wp} \times N_{wp}}$ are the mass, damping and stiffness matrices of the flexible part obtained from FEA, $\boldsymbol{M}_{rr,wp} \in \mathbb{R}^{6\times6}$ corresponds to the mass matrix known from rigid multibody dynamics, $\boldsymbol{M}_{fr,wp} = \boldsymbol{M}_{rf,wp}^T$ couples the elastic deformations and the rigid body movement. The vectors $\boldsymbol{h}_{r,wp}$ and $\boldsymbol{h}_{f,wp}$ collect generalized inertia forces. Using a lumped mass formulation, all quantities needed to form Eq. (3) can be calculated from FEA results, [4]. The vector $\boldsymbol{f}_{e,wp}$ collects external forces acting on the nodal degrees of freedom. Here, this is the process force $\boldsymbol{F}_p$ that acts at the TCP, thus

$$\boldsymbol{f}_{e,wp} = \boldsymbol{B}_{p,wp} \cdot \boldsymbol{F}_p. \tag{4}$$

The input matrix $\boldsymbol{B}_{p,wp}$ projects hereby the process force on the elastic dofs of the workpiece that correspond to the TCP. Due to rotation and feed, the force application point is not constant but varies with time. The input

matrix is therefore a function of the rigid body motion of workpiece and tool,

$$\boldsymbol{B}_{p,wp} = \boldsymbol{N}_{wp}(\boldsymbol{x}_{r,wp}, \boldsymbol{x}_{r,t}). \tag{5}$$

Figure 4 shows the general case where the force application point is not coincident with a node of the underlying FE-mesh of the cylinder surface. The force $\boldsymbol{F}_p$ has to be expressed via forces acting on the dofs of the adjacent nodes h,i,j and k. This is done by means of bilinear shape functions using local distances ξ and η. The matrix $\boldsymbol{N}_{wp}$ contains nonzero entries only on positions corresponding to the dofs of nodes h,i,j and k.

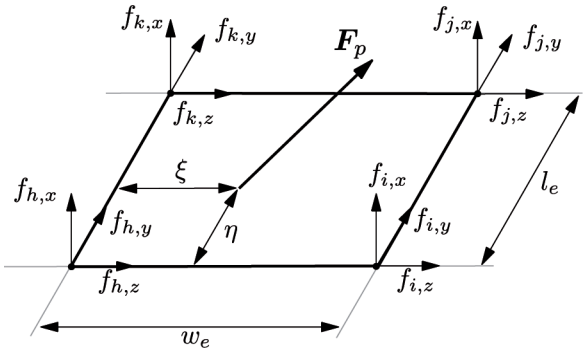

Fig. 4. Cutting force acting on a surface element

The displacements of the workpiece at the TCP $\boldsymbol{y}_{p,wp}$ are expressed using the output matrix $\boldsymbol{C}_{p,wp}$, $\boldsymbol{y}_{p,wp} = \boldsymbol{C}_{p,wp} \cdot \boldsymbol{x}_{f,wp}$. As $\boldsymbol{y}_{p,wp}$ is the displacement on the force application point, it becomes clear that $\boldsymbol{C}_{p,wp}$ also depends on the rigid dofs of workpiece and tool,

$$\boldsymbol{C}_{p,wp} = \boldsymbol{N}_{wp}^{T}(\boldsymbol{x}_{r,wp}, \boldsymbol{x}_{r,t}) \cdot \boldsymbol{x}_{f,wp} \ , \tag{6}$$

using the same shape functions.

2.3. Mode Synthesis Method

Typically, in order to get accurate results from FEA, a fine mesh is used, resulting in a high number of elements. Correspondingly, the number of nodes is high. Consequently, the equations of motion of the flexible model in the form described by Eqs. (3) and (1) contain a high number of generalized coordinates. This number is in general too high to allow for an efficient numerical implementation. This problem is overcome with the help of model order reduction techniques that allow to reduce the number of generalized coordinates while maintaining a reasonable accuracy of the results.

In this work, the mode synthesis method using modes of vibration is used. The nodal displacements $\boldsymbol{x}_f$ of workpiece and tool are hereby expressed in terms of modal coordinates $\boldsymbol{q}$ using the coordinate transformation

$$\boldsymbol{u} = [\phi_{m,1} \ldots \phi_{m,N}] \cdot \boldsymbol{q} = \boldsymbol{\Phi}_m \cdot \boldsymbol{q} \ . \tag{7}$$

The modal coordinates $\boldsymbol{q}$ represent the contribution of the displacement field given by the modal matrix $\boldsymbol{\Phi}_m$ towards the nodal degrees of freedom. A modal coordinate q_i belongs to the mode of vibration $\boldsymbol{\phi}_{m,i}$ associated to a natural frequency $\omega_{m,i}$ of the flexible body. Eigenfrequencies and -vectors can be obtained by solving the eigenvalue problem,

$$(\boldsymbol{M}_{ff}\omega_{m,i}^2 - \boldsymbol{K}_{ff}) \cdot \phi_{m,i} = \boldsymbol{0} \ . \tag{8}$$

Often only a fraction of the modes is needed to accurately describe the system behaviour. Consequently, the columns corresponding to the other modes are excluded from $\boldsymbol{\Phi}$. The mode synthesis technique allows thus to improve the numerical efficiency.

2.4. Process Force Model

Material removal operations represent complex physico-chemical processes involving a multitude of different effects. Those range from high plasticity and elevated deformation rates of the material to extreme heat gradients and interactions between tool and workpiece like abrasion and pressure wielding. Precise accounting for these effects would impose very high demands on the process model. In general, it is therefore customary to factor the process by empirically determined force laws.

In this work, we consider experimentally determined force laws that were first introduced by Kienzle and Victor [5]. They investigated the acting forces during the turning of different materials for a given nominal process. They were thus able to derive laws of the form

$$F_i = k_i a_p h \tag{9}$$

for the three components of the process force, the cutting force F_c, the passive force F_p and the feed force F_f. Each of the components was assumed to be proportional to the chip geometry, i.e. the product of chip thickness h and the depth of cut a_p. The chip thickness relates to the feed movement of the tool, the depth of cut is the tool movement perpendicular to the surface.

However, they soon discovered that (9) only holds for small variations around their nominal process conditions. Correction factors were added resulting in highly nonlinear force laws.

For stability analysis, it is sufficient to observe small force variations around the cutting conditions that are to be analyzed. In this work, we therefore consider a linear force law $\boldsymbol{F}_p = [F_p\ F_c\ F_f] = \boldsymbol{k}_{a_p}(a_p(t)-a_{p,0})+\boldsymbol{k}_h(h(t)-h_0)+\boldsymbol{F}_0$, obtained through linearization around a nominal depth of cut $a_{p,0}$ and chip thickness h_0 that lead to the constant force $\boldsymbol{F}_0$. Extensive data on specific cutting forces and correction factors can be taken from literature, e.g. from [6].

The force law is reformulated and the width and thickness variation expressed by the workpiece and tool displacements $\boldsymbol{y}_{p,wp}$, $\boldsymbol{y}_{p,t}$ at the tool center point. Because successive cuts usually overlap in turning, the force not only depends on the present, but also on past values of workpiece and tool displacements, modeled by the discrete delay $\tau = 2\pi/\omega$, resulting in

$$\boldsymbol{F}(t) = \boldsymbol{F}_0 + \boldsymbol{G}\cdot(\underbrace{\boldsymbol{y}_t(t)+\boldsymbol{y}_{wp}(t)}_{\boldsymbol{u}_{tcp}(t)} - \mu\boldsymbol{u}_{tcp}(t-\tau))\ . \tag{10}$$

The factor μ comprised between 0 and 1 is used to describe the overlapping of consecutive cuts. The matrix $\boldsymbol{G}$ contains the specific cutting forces and projects the TCP-movements in the directions of depth and width of cut.

2.5. Coupled System

Here, rotational velocities between 600 and 1000 rpm will be considered, corresponding to time delays ranging from 0.1 to 0.06 seconds. Higher rotational velocities are not permitted because of limitiations of the allowable cutting speeds by the equipment. The rotational velocity is constant during the operation, the accelerations of the floating frame of reference of the workpiece therefore vanish. The equations of motion of the workpiece (3) can thus be simplified. Coupling with the tool equations using the force law (10) and the in- and output matrices (6) and (5) yields the coupled equations of motion of workpiece and tool,

$$\boldsymbol{M}\cdot\ddot{\boldsymbol{x}}_f(t)+\boldsymbol{D}\cdot\dot{\boldsymbol{x}}_f(t)+(\boldsymbol{K}+\boldsymbol{K}_{cp}(t))\cdot\boldsymbol{x}_f(t)+\mu\boldsymbol{K}_{cp}(t)\cdot\boldsymbol{x}_f(t-\tau) = \boldsymbol{B}\cdot[\boldsymbol{F}(t)\ \ u(t)], \tag{11}$$

where

$$\boldsymbol{M} = \begin{bmatrix}\boldsymbol{M}_{f,wp} & \boldsymbol{0}\\ \boldsymbol{0} & \boldsymbol{M}_{f,t}\end{bmatrix} \qquad \boldsymbol{D} = \begin{bmatrix}\boldsymbol{D}_{f,wp} & \boldsymbol{0}\\ \boldsymbol{0} & \boldsymbol{D}_{f,t}\end{bmatrix},$$

$$\boldsymbol{K} = \begin{bmatrix}\boldsymbol{K}_{f,wp} & \boldsymbol{0}\\ \boldsymbol{0} & \boldsymbol{K}_{f,t}\end{bmatrix}, \qquad \boldsymbol{B} = \begin{bmatrix}\boldsymbol{B}_{p,wp}(t) & \boldsymbol{0}\\ \boldsymbol{B}_{p,t} & \boldsymbol{B}_{u,t}\end{bmatrix},$$

$$\boldsymbol{K}_{cp} = \begin{bmatrix}\boldsymbol{B}_{p,wp}(t)\cdot\boldsymbol{G}\cdot\boldsymbol{C}_{p,wp}(t) & \boldsymbol{B}_{p,wp}(t)\cdot\boldsymbol{G}\cdot\boldsymbol{C}_{p,t}\\ \boldsymbol{B}_{p,t}\cdot\boldsymbol{G}\cdot\boldsymbol{C}_{p,wp}(t) & \boldsymbol{B}_{p,t}\cdot\boldsymbol{G}\cdot\boldsymbol{C}_{p,t}\end{bmatrix}, \quad \boldsymbol{x}_f = \begin{bmatrix}\boldsymbol{x}_{f,wp}\\ \boldsymbol{x}_{f,t}\end{bmatrix}.$$

The derived nonlinear model is subsequently used to analyze the dynamic stability of the turning process. A feedback law using the available measurements is then implemented and the effects on the stability boundary are compared.

3. Stability analysis

Consecutive cuts on the same surface, modeled in Eq. (10) as an interaction of the time-delay of the system and the system dynamics, can lead to self-excited vibrations. These instabilities cause a poor surface finish and can even damage the equipment. In practical application, the operator would always seek to chose the operation parameters such that no instabilities occur. This is done by use of the expertise of the operator as well as the help of so-called stability charts. Those charts display the domain of stable and unstable cutting in a 2D plot parametrized by modifiable process parameters. For turning, these are usually the rotational velocity of the workpiece in revolutions per minute (rpm) and depth or width of cut. As the flexibility of workpiece and tool in depth of cut direction is considerably higher than in chip thickness direction, Eq. (10) will be slightly rewritten and only the variation in depth of cut direction considered,

$$\Delta \boldsymbol{F} = \boldsymbol{V} k_{pf} \delta a_p = \boldsymbol{G} \cdot (\boldsymbol{u}_{tcp}(t) - \mu \boldsymbol{u}_{tcp}(t-\tau))) \ . \tag{12}$$

Furthermore, as the focus of this contribution lies on improving dynamic stability, the charts will be given in terms of rotational velocity ω and the force parameter k_{pf}. This simplifies the evaluation of the results. Using the extensive data available in literature, [6], k_{pf} can be related to the modifiable parameters for a known process. The force direction $\boldsymbol{V}$ is consequently a unity vector.

The coupled equations of motion of tool and workpiece (11) form together with the cutting force law (10) a system of nonlinear delay differential equations. Analysis of its stability is a difficult task that has received and still receives a lot of interest in the scientific community. Different analysis methods have been proposed that differ greatly in their applicability. The methods available can be distinguished in three different classes, i.e. frequency domain based methods, methods using an approximation as a time-discrete system and time-domain simulations.

Methods based on an approximation as a time discrete system deduce the stability of a linear periodic time varying system with the help of the eigenvalues of the transition matrix of an approximating discrete system. Whilst they do not allow to find an analytical solution for the stability boundary as the frequency dependent methods do, [7], they offer a much faster calculation

and a more robust determination of stability than time domain simulations. In addition, they allow to account for the time-varying dynamics of the system and are, therefore, the method of choice here. They have been applied successfully in different applications [8,9].

Starting point for this class of methods is Floquet Theory, [10]. Floquet Theory states that the stability of a time-variant periodic system can be deduced by means of the largest eigenvalue of the corresponding transition matrix. Although Floquet Theory can be generalized for functional differential equations and, therefore, applied to systems with time delay, practical application is not straightforward. One reason is, that the rate of change of a delayed system depends not only on the present, but also on the past of the system. Its corresponding state-space representation and thus the fundamental matrix are therefore infinite-dimensional. To obtain a finite-dimensional map of the infinite-dimensional system, several strategies exist. The most popular are the Temporal Finite Element Method, [11,12], and the Semi-Discretization Method, [3,13].

Both methods focus on finding a discrete map of the continuous system. What is determined is thus the transition between two successive states ζ_d and ζ_{d+1} of the approximated discrete system,

$$\zeta_d = \mathbf{\Phi} \cdot \zeta_{d+1} \ , \tag{13}$$

as illustrated in Figure 5.

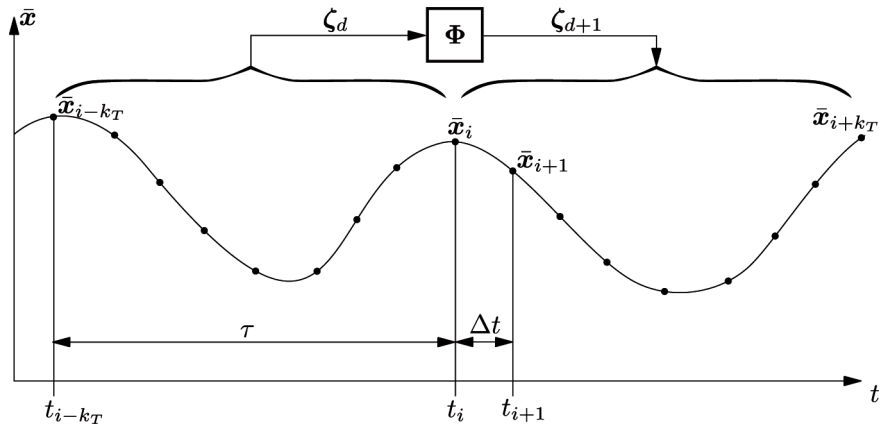

Fig. 5. Discretization of the system past and approximation as time-discrete system

Here, these are equivalent to two successive rotations of the workpiece. The state of the discrete system consists of the current state of the system as well as a finite number of past states at given instants,

$$\zeta_d = [\bar{\boldsymbol{x}}_i \ \ \bar{\boldsymbol{x}}_{i-1} \ \ \cdots \ \ \bar{\boldsymbol{x}}_{i-k_T}], \qquad \zeta_{d+1} = [\bar{\boldsymbol{x}}_{i+k_T} \ \ \bar{\boldsymbol{x}}_{i+k_T-1} \ \ \cdots \ \ \bar{\boldsymbol{x}}_i], \tag{14}$$

Having calculated the transition matrix $\mathbf{\Phi}$, the stability of the approximated system can be determined by means of the largest eigenvalue of $\mathbf{\Phi}$. For a stable system, they have to be located inside the unit circle of the complex plane,

$$|\lambda(\mathbf{\Phi})|_{\max} = \begin{cases} > 1 & \text{unstable,} \\ = 1 & \text{boundary of stability,} \\ < 1 & \text{stable.} \end{cases} \tag{15}$$

The Semi-Discretization-Method will subsequently be used to derive an approximation as a time discrete system and construct the corresponding transition matrix. The procedure follows the outline given in [14].

Starting point for the method is a state-space representation of the form

$$\dot{\bar{\boldsymbol{x}}} = \boldsymbol{A}(t) \cdot \bar{\boldsymbol{x}}(t) + \boldsymbol{Q}(t) \cdot \bar{\boldsymbol{x}}(t-\tau) \ . \tag{16}$$

The matrices $\boldsymbol{A}$ and $\boldsymbol{Q}$ are hereby supposed to be time-variant and periodic,

$$\boldsymbol{A}(t+T) = \boldsymbol{A}(t), \quad \boldsymbol{Q}(t+T) = \boldsymbol{Q}(t) \ .$$

Note that the periodicity T in the considered case equals the time delay τ. When the feed movement is neglected, the overlap factor becomes $\mu = 1$ and the time-varying terms in Eq. (11) are indeed periodic. This simplification is justified, because the tool moves here only a small fraction of the length of the cutting edge during one rotation. The matrices $\boldsymbol{A}$ and $\boldsymbol{Q}$ can then be written as

$$\boldsymbol{A}(t) = \begin{bmatrix} \boldsymbol{0} & \boldsymbol{E} \\ \boldsymbol{M}^{-1} \cdot (\boldsymbol{K} + \boldsymbol{K}_{cp}(t)) & \boldsymbol{M}^{-1} \cdot \boldsymbol{D} \end{bmatrix}, \quad \boldsymbol{Q}(t) = \begin{bmatrix} \boldsymbol{0} & \boldsymbol{0} \\ \boldsymbol{M}^{-1} \cdot \boldsymbol{K}_{cp}(t) & \boldsymbol{0} \end{bmatrix}, \tag{17}$$

and the state vector reads

$$\bar{\boldsymbol{x}} = [\boldsymbol{x}_f \ \ \dot{\boldsymbol{x}}_f]^T \ . \tag{18}$$

The submatrix $\boldsymbol{E}$ is hereby an identity matrix with appropriate dimensions. Departing from an instant t_i in time, the system past is represented by means of discrete interpolation points

$$\bar{\boldsymbol{x}}_{i-j} = \bar{\boldsymbol{x}}(t_i - j\Delta t), \tag{19}$$

the discrete time step Δt is hereby chosen such that

$$k_T \Delta t = T, \qquad k_T \in \mathbb{N} \ . \tag{20}$$

For the interval $[t_i \ \ t_{i+1}]$, the delayed states $\bar{\boldsymbol{x}}(t-\tau)$ are approximated by a constant value. The value at the middle of the interval is chosen and expressed by weighted means of the closest interpolation points

$$\bar{\boldsymbol{x}}(t-\tau) \approx \bar{\boldsymbol{x}}(t + \Delta t/2 - \tau) \approx w_b \bar{\boldsymbol{x}}_{i-k_T} + w_a \bar{\boldsymbol{x}}_{i-k_T+1} \ . \tag{21}$$

The weighting coefficients are set to $w_a = w_b = 0.5$. The time variant coefficient matrices $\boldsymbol{A}$ and $\boldsymbol{Q}$ are approximated in a similar way,

$$\boldsymbol{A}(t) \approx \boldsymbol{A}(t + \Delta t/2) =: \boldsymbol{A}_i, \qquad \boldsymbol{Q}(t) \approx \boldsymbol{Q}(t + \Delta t/2) =: \boldsymbol{Q}_i \ . \tag{22}$$

The initial delay differential equation is thus approximated on the interval $[t_i \ t_{i+1}]$ by the ordinary differential equation

$$\dot{\bar{\boldsymbol{x}}} = \boldsymbol{A}_i \cdot \bar{\boldsymbol{x}} + \boldsymbol{Q}_i \cdot (w_a \bar{\boldsymbol{x}}_{i-k_T+1} + w_b \bar{\boldsymbol{x}}_{i-k_T}) \ . \tag{23}$$

For a given initial condition $(\bar{\boldsymbol{x}}_i, \bar{\boldsymbol{x}}_{i-k_T}, \bar{\boldsymbol{x}}_{i-k_T+1})$, the state $\bar{\boldsymbol{x}}_{i+1}$ at the end of the interval can be obtained by integrating this equation,

$$\begin{aligned} \bar{\boldsymbol{x}}_{i+1} &= e^{(\boldsymbol{A}_i \cdot \Delta t)} \cdot \bar{\boldsymbol{x}}_i + (e^{(\boldsymbol{A}_i \Delta t)} - \boldsymbol{E}) \cdot \boldsymbol{A}_i^{-1} \cdot \boldsymbol{Q}_i \cdot (w_a \bar{\boldsymbol{x}}_{i-k_T} + w_b \bar{\boldsymbol{x}}_{i-k_T+1}) \\ &= \boldsymbol{P}_i \cdot \bar{\boldsymbol{x}}_i + \boldsymbol{S}_i \cdot \bar{\boldsymbol{x}}_{i-k_T} + \boldsymbol{R}_i \cdot \bar{\boldsymbol{x}}_{i-k_T+1}. \end{aligned} \tag{24}$$

The solution for the interval T, i.e. one complete revolution of the tool, can be obtained based on the solutions of all the subintervals. Two ways exist to build the transition matrix $\boldsymbol{\Phi}$. Following the presentation in [3,13] a transition matrix $\bar{\boldsymbol{\Phi}}_m$ can be constructed for each of the k_t timesteps Δt that gives the transition from the beginning to the end of the subinterval. The transition matrix for the entire period T is then obtained by multiplying the $\bar{\boldsymbol{\Phi}}_m$. In the considered case of turning, the number of subintervals is high due to the relatively long time delay (compared with the milling operation considered in the reference). The, therefore, elevated number of matrix multiplications is computationally intensive. To avoid those multiplications, a calculation method is adopted that is referred in [14] as the direct method (in contrast to the successive multiplication).

Writing Eq. (24) for each of the subintervals in matrix form gives

$$\underbrace{\begin{bmatrix} \boldsymbol{E} & -\boldsymbol{P}_{i+k_T-1} & \boldsymbol{0} & \boldsymbol{0} & \cdots & \boldsymbol{0} & \boldsymbol{0} & \boldsymbol{0} \\ \boldsymbol{0} & \boldsymbol{E} & -\boldsymbol{P}_{i+k_T-2} & \boldsymbol{0} & \cdots & \boldsymbol{0} & \boldsymbol{0} & \boldsymbol{0} \\ \vdots & \ddots & \ddots & \ddots & \ddots & \ddots & \vdots & \vdots \\ \boldsymbol{0} & \boldsymbol{0} & \boldsymbol{0} & \boldsymbol{0} & \cdots & \boldsymbol{0} & \boldsymbol{E} & -\boldsymbol{P}_i \\ \boldsymbol{0} & \boldsymbol{0} & \boldsymbol{0} & \boldsymbol{0} & \cdots & \boldsymbol{0} & \boldsymbol{0} & \boldsymbol{E} \end{bmatrix}}_{=: \boldsymbol{\Phi}_l} \cdot \begin{bmatrix} \bar{\boldsymbol{x}}_{i+k_t} \\ \bar{\boldsymbol{x}}_{i+k_t-1} \\ \cdots \\ \bar{\boldsymbol{x}}_{i+1} \\ \bar{\boldsymbol{x}}_i \end{bmatrix}$$

$$= \underbrace{\begin{bmatrix} \boldsymbol{S}_{i+k_T-1} & -\boldsymbol{T}_{i+k_T-1} & \boldsymbol{0} & \boldsymbol{0} & \cdots & \boldsymbol{0} & \boldsymbol{0} & \boldsymbol{0} \\ \boldsymbol{0} & \boldsymbol{S}_{i+k_T-2} & -\boldsymbol{T}_{i+k_T-2} & \boldsymbol{0} & \cdots & \boldsymbol{0} & \boldsymbol{0} & \boldsymbol{0} \\ \vdots & \ddots & \ddots & \ddots & \ddots & \ddots & \vdots & \vdots \\ \boldsymbol{0} & \boldsymbol{0} & \boldsymbol{0} & \boldsymbol{0} & \cdots & \boldsymbol{0} & \boldsymbol{S}_i & -\boldsymbol{T}_i \\ \boldsymbol{0} & \boldsymbol{0} & \boldsymbol{0} & \boldsymbol{0} & \cdots & \boldsymbol{0} & \boldsymbol{0} & \boldsymbol{0} \end{bmatrix}}_{=: \boldsymbol{\Phi}_r} \cdot \begin{bmatrix} \bar{\boldsymbol{x}}_i \\ \bar{\boldsymbol{x}}_{i-1} \\ \cdots \\ \bar{\boldsymbol{x}}_{i-k_T+1} \\ \bar{\boldsymbol{x}}_{i-k_T} \end{bmatrix} . \tag{25}$$

The matrix $\boldsymbol{\Phi}$ can then be obtained as

$$\zeta_d = \underbrace{\boldsymbol{\Phi}_l^{-1} \cdot \boldsymbol{\Phi}_r}_{\boldsymbol{\Phi}} \cdot \zeta_{d+1} \ . \tag{26}$$

In order to calculate the largest eigenvalue, the eigenvalue problem

$$(\boldsymbol{\Phi}_l^{-1} \cdot \boldsymbol{\Phi}_r - \lambda \boldsymbol{E}) \cdot \boldsymbol{U} = \boldsymbol{0} \tag{27}$$

needs to be solved. The equivalent generalized eigenvalue problem

$$(\boldsymbol{\Phi}_r - \lambda \boldsymbol{\Phi}_l) \cdot \boldsymbol{U} = \boldsymbol{0} \tag{28}$$

is considered to avoid the costly calculation of the inverse. Note that Eqs. (27) and (28) have the same eigenvalues. The largest eigenvalue of the above equation can be efficiently determined using the QZ-algorithm that is readily available in *matlab*.

Note that Eq. (28) allows to conclude on the stability of one specific system. In order to calculate the boundary of stability, the criterion must be evaluated for different values of k_{pf} and τ. To reduce the number of evaluations, an adaptive mesh refinement is used.

4. Feedback control to improve dynamic stability

To improve the dynamic behavior of the turning operation, a feedback control using the adaptronic turning chisel is synthesized and tested in simulation. The criterion to judge the obtained results is hereby given by the stability analysis procedure presented in the previous section. The domain of stable cutting is to be increased. Typically, actuators and sensors are only effective up to a certain frequency. A good feedback control exhibits thus a roll-off at high frequencies. This also increases the robustness with respect to faster dynamics that have been neglected in the design of model based controllers.

The tool is also part of a larger system that seeks not only to prevent unstable cutting, but also compensates shape errors typical for turning of thin-walled cylinders, [15]. As part of this system, the tool must also execute precise infeed movements. An additional demand is thus good reference tracking in the low frequency domain. In this contribution, however, the focus lies on stability improvement. The demand is thus not explicitly taken into account, but kept in mind when discussing the concepts.

Four different concepts will be implemented and compared. The first two, Direct-Velocity-Feedback (DVF) and Positive-Position-Feedback (PPFB), are collocated control concepts using either a velocity or a position feedback. They are usually found in the context of active vibration damping of structures and need no system model. The next two, the Frequency-Shaped-Linear-Quadratic-Regulator (FS-LQR) and H_∞-optimal control are model based concepts that synthesize a controller that is optimal in the sense of a given criterion. The potential of adaptronic machine tools in combination with collocated and model-based control concepts has been shown in previous studies, [16,17].

4.1. Collocated control

Collocated control concepts, [18,19], introduce damping locally. The control laws are simple and do not require a model of the system. They depend on very few parameters that can easily be tuned manually. In the ideal case, they guarantee stability for a stable system, i.e. they do not destabilize it. Collocated control concepts are thus a good first choice for control problems involving vibrations. If a reference signal needs to be tracked, an additional outer or high authority control loop must be designed.

Collocated control demands that actuators and sensors are collocated, i.e. they have to be located at the same place and must be energetically conjugated. A force input is thus calculated based on a displacement or velocity measurement obtained at the same point. In the case of the adaptronic tool holder of Figure 2, the force created by the piezo stack is collocated with the measurement of the piezo elongation x_p obtained through the eddy current sensor. The most straightforward dissipative force law uses a velocity feedback,

$$u = -d_v \dot{x}_p \ , \tag{29}$$

effectively making the actuator act like a damper. Collocated control using Eq. (29) is referred to as Direct-Velocity-Feedback (DVF). To improve the

roll-off of the control system and avoid high frequency excitation, the position signal is filtered by a first order low pass filter W_{dvf},

$$W_{dvf} = \frac{\omega_f}{s + \omega_f}. \tag{30}$$

The filter frequency ω_f is chosen according to the frequency of the mode to be controlled.

Using directly the piezo stack elongation and a positive feedback leads to a feedback law called Positive-Position-Feedback (PPFB),

$$u = k_c x_p \ . \tag{31}$$

In order to improve the roll-off of the control system, the position signal is filtered by a second order low pass filter,

$$W_{ppfb}(s) = \frac{\omega_f^2}{s^2 + 2\xi_f \omega_f s + \omega_f^2}. \tag{32}$$

As before, the filter frequency ω_f is hereby set close to the frequency of the mode that is to be controlled. The filter is heavily damped, e.g. $\xi_f = 0.7$. It should be noted that the PPFB causes a local stiffness reduction. The system can therefore be destabilized if the open-loop static gain is unity.

It is to be expected that the use of a collocated control concept is somehow limited here by the relatively long distance between the actuator input and the TCP. Model based concepts promise here to have advantages as using a system model allows to globally affect the system dynamics using the local force input and sensor information.

4.2. The Frequency-Shaped-Linear-Quadratic-Regular

The first model based concept, the FS-LQR, is an optimal state feedback using a frequency dependent cost functional. It is also widely used in the field of control of flexible structures, [18,19], and an extension of the classical LQR. The LQR is an optimal state feedback calculated to minimize the quadratic performance criterion

$$J = \int_0^\infty [\tilde{\boldsymbol{x}}^T(t) \cdot \boldsymbol{Q} \cdot \tilde{\boldsymbol{x}}(t) + u(t) r u(t)] dt, \tag{33}$$

where the positive semi-definite matrix $\boldsymbol{Q}$ and the positive coefficient r are used to weight the system states $\tilde{\boldsymbol{x}}$ and the control input u. For a system in modal form, i.e. when the system has been transformed and/or reduced using

Eq. (7), the states represent modal amplitudes and velocities. Choosing $\boldsymbol{Q}$ as a diagonal matrix allows to directly penalize specific modes, effectively increasing the damping of the selected mode.

Directly using constant weighting matrices can, however, destabilize the modes that have been neglected in the controller design. This phenomenon, called spillover, can be prevented by using frequency dependent weighting matrices. According to Parseval's theorem, the cost functional (33) can be transformed into the frequency domain,

$$J = \frac{1}{2\pi} \int_0^\infty [\tilde{\boldsymbol{x}}^*(\omega) \cdot \boldsymbol{Q} \cdot \tilde{\boldsymbol{x}}(\omega) + u^*(\omega) r u(\omega)] d\omega. \tag{34}$$

The symbol * is used to denote the hermitian, i.e. the complex conjugate transposed. If the system output is given by $y = \boldsymbol{C} \cdot \tilde{\boldsymbol{x}}$, using frequency depending weighting matrices of the form

$$\boldsymbol{Q}(\omega) = \boldsymbol{C}^* h(\omega)^* h(\omega) \boldsymbol{C}, \quad r(\omega) = R s^*(\omega) s(\omega) \tag{35}$$

is equivalent to adding input and output filters to the system and minimizing the frequency independent cost functional

$$J = \int_0^\infty [y_f^* y_f + u_f^* r u_f] d\omega = \int_0^\infty [y_f^2 + u_f^2 r] dt. \tag{36}$$

The state feedback,

$$u = -\boldsymbol{K} \cdot \tilde{\boldsymbol{x}}_n, \tag{37}$$

that minimizes (36) can now be obtained by solving the LQR-problem for the system augmented with the filters. The new system state is

$$\tilde{\boldsymbol{x}}_n = [\boldsymbol{x}_i \;\; \tilde{\boldsymbol{x}} \;\; \boldsymbol{x}_o]^T \,, \tag{38}$$

with $\tilde{\boldsymbol{x}}$ being the state vector of the original system and $\boldsymbol{x}_i$, $\boldsymbol{x}_o$ the states of the input and output filters. It should be noted, that the LQR problem can easily be augmented to satisfy tracking requirements.

Figure 6a shows the schematic view of the entire controller, including the input and output filters. Typically, the system states cannot be measured in their entirety but must be reconstructed from the available measurements using an observer, e.g. a Kalman Filter. Because the filters are calculated in the computer, their states are known and need not be reconstructed. Figure 6b shows the filter characteristics adopted here. The output filter puts more weight on low frequency, the input filter penalizes high frequency control signals. The parameter R will serve as design parameter. The acceleration measurement has been chosen as output to be filtered.

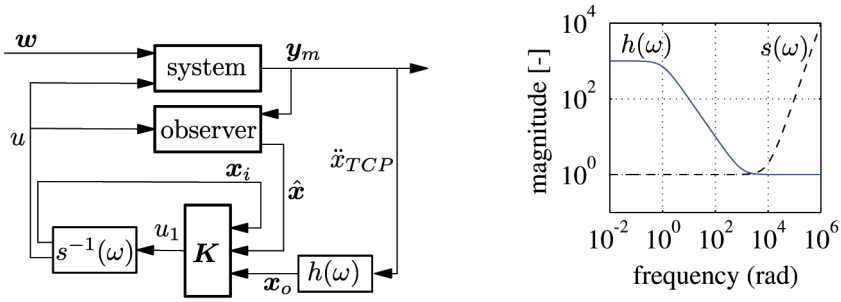

(a) Structure of the frequency shaped LQG, observer and system with filters

(b) Frequency dependent weighting functions for LQR

Fig. 6. Structure and filter functions of the FS-LQG

4.3. H_∞ control

H_∞ control belongs to the so called robust control techniques. Modern robust control techniques, [20,21], allow to define the desired closed loop behavior more precisely by "shaping" the closed loop transfer functions. First, the control problem needs to be expressed by means of the generalized plant $\boldsymbol{P}$ and signals $\boldsymbol{w}$, $\boldsymbol{u}$, $\boldsymbol{z}$ and $\boldsymbol{v}$. A block diagram is shown in Figure 7.

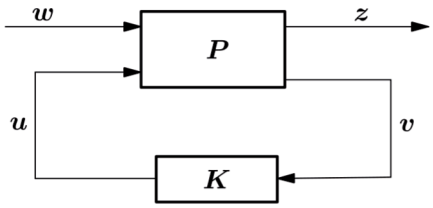

Fig. 7. Generalized plant $\boldsymbol{P}$ and controller $\boldsymbol{K}$

The vector of exogenous signals $\boldsymbol{w}$ collects hereby all external quantities acting on the system, such as references and disturbances, $\boldsymbol{z}$, the performance measurement, contains signals that allow to assess the system behaviour. The controlled inputs $\boldsymbol{u}$ and measurements $\boldsymbol{v}$ group the available inputs and sensor outputs of the system. When $\boldsymbol{P}$ is known, the problem of controller synthesis is formulated as an optimization problem. Find a stabilizing controller $\boldsymbol{K}$ such that the norm of the transfer function of the closed loop from $\boldsymbol{w}$ to $\boldsymbol{z}$ is minimized. In the case of H_∞ control,

$$\|F_l(\boldsymbol{P},\boldsymbol{K})\|_\infty = \gamma \stackrel{!}{=} \min \quad . \tag{39}$$

Here, F_l denotes a lower linear fractional transformation of $\boldsymbol{P}$ with $\boldsymbol{K}$ as parameter, i.e. $F_l(\boldsymbol{P},\boldsymbol{K})$ is obtained by using $\boldsymbol{K}$ to close the loop shown in Figure 7. The optimization problem is usually solved using linear matrix

inequalities or algebraic riccatti equations. Solvers are readily available in programs like *matlab*. They return the optimal controller $\boldsymbol{K}$ and the minimal value γ of the criterion.

Usually, $\boldsymbol{u}$ and $\boldsymbol{v}$ are given by the system to be controlled and can not be changed. The task of the control engineer is thus to define the signals $\boldsymbol{w}$ and $\boldsymbol{z}$ to suit the needs of the given problem. Those signals are usually filtered to achive a desired behaviour of the resulting controller. Figure 8a shows the choice used here. The tracking error ϵ between the infeed of the tool and some given reference is included, as well as the control signal. An unknown perturbation acting on the TCP is added to force optimization with respect to disturbances ocurring during machining. The filters $W_1(s)$ and $W_2(s)$ are first order stable transfer functions, W_3 is a constant gain. The reference and control signals are scaled such that a signal of magnitude 1 represents a large signal, i.e. a piezo force of $10000N$ and a reference command of 10μm.

Filters $W_1(s)$ can be used to directly shape the transfer function from the reference to the error of the closed loop, that is called the sensitivity $S(s)$. To ensure a small tracking error, usually $S(s)$ is wanted to be small in the lower frequency range while left unchanged in the higher range. The transfer function $W_2(s)$ allows to influence the complementary sensitivity $T(s)$ of the system. In order to avoid amplification of noise, we want $T(s)$ to be small for high frequencies to penalize high frequency control signals. Figure 8b shows the filters used in the controller design. The minimal value γ of criterion (39) indicates if the constraints imposed by the filters have been respected. If $\gamma < 1$, then $|S(s)| < |1/W_1(s)|$ and $|T(s)| < |1/W_2(s)|$. The constant weight W_3 will subsequently serve as design parameter.

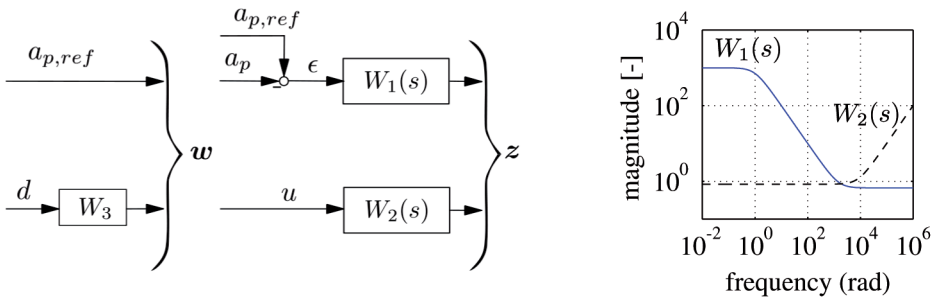

(a) Choice of exogenous inputs and performance outputs and Filters

(b) Weights $W_1(s)$ and $W_2(s)$ for H_∞ controller synthesis

Fig. 8. Choice of signals for generalized plant and filters

5. Numerical Experiments

The adaptronic tool is now coupled with two different workpiece models, the stability of the resulting system analyzed and the effects of the presented control concepts observed. Numerous testing conditions are conceivable that boil all down to two basic cases: The system dynamics is dominated by the tool or it is dominated by the workpiece. The display is limited to those two cases represented by two test systems. System 1 represents hereby the coupling with a moderately thin steel cylinder of wall thickness 6mm. In this case, the workpiece exhibits dimensions that could typically be encountered in a workshop. In system 2, the model of a very thin workpiece of wall thickness 1mm is used. This presents a type of workpiece that is very difficult to machine and that would typically demand the use of specialized clamping devices. The remaining dimensions and material properties are the same for both models and given in Table 1. In both cases, we consider the system immediately after machining has started, i.e. the tool is located at the far end of the cylinder, away from the chuck.

Table 1.

Numerical values for the considered workpiece models

l	d	h_j	β_j	Youngs modulus	density	Poisson's ratio
0.2m	0.12m	10mm	20°	$210 \cdot 10^6$ N/m	7800 kg/m^3	0.3

First of all, the stability diagrams of workpiece and tool are determined independently. For this, each of the workpiece models is coupled with a rigid tool and the tool is coupled with a rigid workpiece. Figure 9b shows the stability boundary of the very thin workpiece and Figure 9a the moderately thin workpiece and the tool. The area under a specific curve is the domain of stable cutting. The stability diagrams were obtained using the Semi-Discretization Method. The number of discretization points for the past state has been chosen to $k_T = 2920$. The analysis was done using a reduced model including the first five modes of workpiece and tool. A further increase of modes or discretization points leads only to minor changes. In fact, the use of four modes and $k_T = 2200$ discretization points already yields the same chart in the case of the workpiece. Two modes are already enough for the tool. From this, it is clear that the instability is due to excitation of the first few modes of the system. The higher frequencies play only a minor role.

The results indicate already that the instability will be due to vibrations of the comparatively long and slender tool in the case of system 1. System 2 will most likely become instable due to vibrations of the very thin workpiece. It should be noted that system 1 can be considered as the typical case in inside turning where flexible tools force the operator to choose lower material

removal rates. System 2, however, is an extreme case that is very difficult to machine.

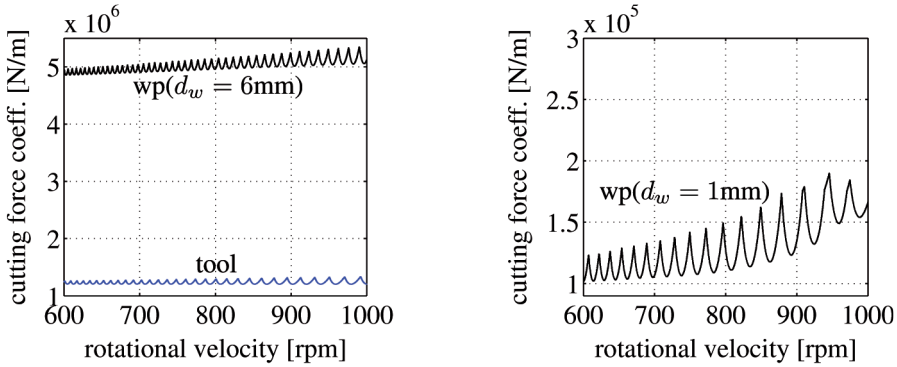

(a) Structure of the frequency shaped LQG, (b) Thin workpiece

Fig. 9. Stability diagrams of the tool and the two different workpiece models

Collocated control concepts are now used to increase the stable domain of system 1. The frequency of the filters for DVF and PPFB is chosen to $\omega_f = 2\pi \cdot 720$, thus roughly equal to the second eigenfrequency of the tool. The gains d_v and k_p of the two concepts are then successively increased and the effect on the stability boundary observed. Figure 10b shows the results of the Positive-Position-Feedback and Figure 10a of the Direct-Velocity-Feedback.

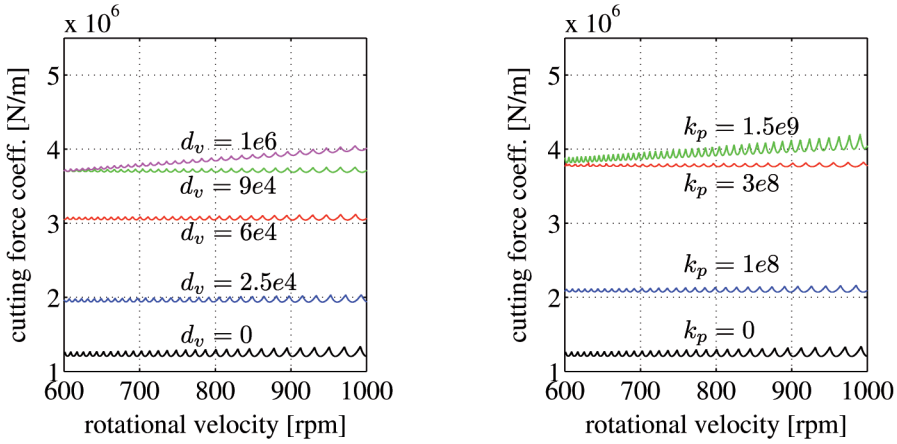

(a) Stability chart of system 1 using Direct-Velocity-Feedback (b) Stability chart of system 1 using Positive-Position-Feedback

Fig. 10. Stability diagrams of system 1 using collocated concepts

Relatively high gains are needed in order to achieve visible results. Higher gains result in a larger domain of stable cutting. Increasing the gains above $d_v = 9 \cdot 10^5$ or $k_p = 3 \cdot 10^8$ results in only minor improvements. It is interesting

to note that those occur mainly in the range of higher rotational velocities. In the case of PPFB, the system can even become unstable independently of the delay when the gain exceeds a value of $k_p = 1.6 \cdot 10^9$ because the stiffness matrix becomes negative definite.

Figure 11a shows the stability diagram of the FS-LQR synthesized using a tool model that includes the first four modes of vibration for different values of the design parameter R. Decreasing R reduces the penalization of the command in Eq. (36). The resulting feedback controller will thus use larger control signals which result in higher damping. This increases the domain of stable cutting. It is interesting to note that there is a value of the weight for which the obtained stability boundary is maximal. Decreasing R below this value does not yield any improvements anymore, but slightly lowers the boundary.

The presented H_∞ controller synthesis method is now tested. As before, a tool model including the first four eigenmodes is used. Figure 11b shows the stability diagrams obtained for different values of W_3. Increasing the parameter W_3 forces the algorithm to consider larger perturbations acting on the TCP and improves the stability of the system. It should be mentioned that the value of γ returned by the controller synthesis algoritm is below one for all displayed values, i.e. the constraints defined by the filters have been respected. The domain of stable cutting is significantly increased. As before, a maximum stability boundary is reached, further increasing W_3 does not yield any improvements. A comparison with chart 9a gives an explanation. For higher values of W_3, the controller stabilizes the tool so well that the stability behaviour becomes dominated by the workpiece. The control law is not able to counteract vibrations of the workpiece, as there is no information about it contained in the model used for controller synthesis.

All previously synthesized controller concepts are now tested with system 2. They are not able to increase the boundary of stability. This could be expected. As they only act on the tool, they do not influence directly the workpiece that is coupled by the process force. To overcome the problem, the model-based concepts can be augmented with a model of the workpiece. The option will be explored using the H_∞ control that performed best in the case of system 1.

Augmenting the system model, however, is made very difficult by the need for a linear, time-invariant model for controller synthesis. The coupling of workpiece and tool is time-dependent due to workpiece rotation and depends on the given process. Furthermore, the workpiece dynamic itself changes during the operation when material is removed.

Figure 12 shows the stability chart of system 2 with and without feedback. Slight improvements were possible choosing the cutting force coefficient

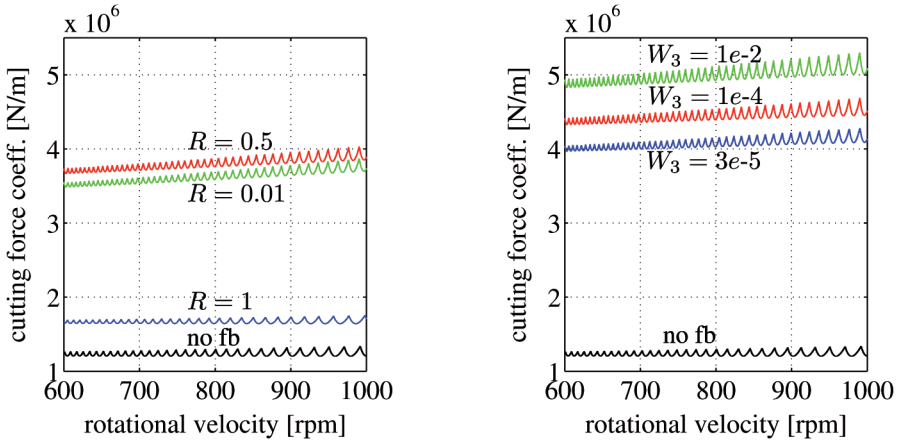

(a) Stability chart of system 1 using the FS-LQR

(b) Stability chart of system 1 using the presented H_∞ controller synthesis method

Fig. 11. Stability diagrams of system 1 using model based concepts

close to the value on the stability boundary. However, the result is sensitive to variations of the coupling coefficient. Classical feedback is not able to improve the turning operation when the dynamic behaviour is dominated by the workpiece.

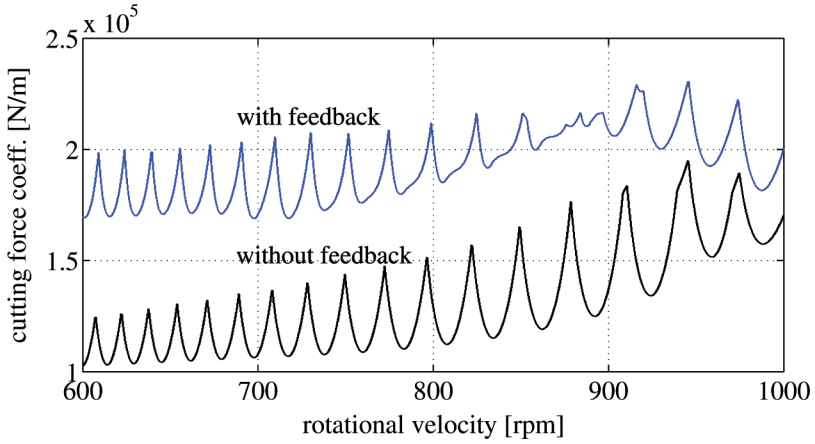

Fig. 12. Stability diagram of thin workpiece and tool with and without feedback

6. Conclusions

The use of an active tool can improve the stability of the system and allows thus to increase machining speed without loss of quality. When the focus lies on damping vibrations and the dynamic behaviour is dominated by the

tool, simple collocated concepts like Direct-Velocity-Feedback and Positive-Position-Feedback can already lead to good results. They introduce damping locally into the system and are thus limited by the location of actuators and sensors and the simple control laws used. The Frequency-Shaped-Linear-Quadratic-Regulator achieved comparable improvements in the numerical experiments. This is somehow dissapointing as it was expected that the use of a system model and an additional measurement allows to obtain results superior to the collocated concepts. The reason is most likely the choice of the criterion (36). It is to be expected that choosing a different weighting of the states can lead to a controller that is capable of further improvements.

The full potential of model based concepts was shown by the presented H_∞ controller. Directly shaping the closed loop transfer functions allows to easily implement additional demands like small tracking errors in the low frequency domain and a limit on the maximum actuator force. The H_∞ controller obtained the best results and was able to prevent instabilities of the tool to such an extent, that vibrations of the workpiece became the main reason for dynamic instability.

When the dynamic behavior is dominated by the cylinder, i.e. with decreasing wall thickness, collocated control concepts fail to improve the stability at all. Model based concepts can still obtain some results when the coupling between workpiece and tool is accounted for in the controller design model. The improvements are however small and sensitive to changes in the coupling coefficients. Linear, time-invariant control laws are not the answer for this special case. The improvement of workpiece dominated dynamic stability is a demanding topic that pends further study.

Acknowledgements

The authors wish to thank Prof. Heisel and his coworkers from the Institute for Machine Tools at the University of Stuttgart. This project is partially funded by the BW-Stiftung. Future support comes from the Cluster of Excellence in Simulation Technology, SimTech, at the University of Stuttgart. All this support is highly appreciated.

Manuscript received by Editorial Board, October 10, 2011;
final version, November 11, 2011.

REFERENCES

[1] Tobias S.A.: Machine-Tool Vibration. London, Blackie and Sons, 1965.
[2] Shabana A.A.: Dynamics of Multibody Systems. Cambridge, Cambridge University Press, 1998.

[3] Insperger T., Stépán G.: Semi-Discretization Method for Delayed Systems. International Journal for Numerical Methods in Engineering, Vol. 55, pp. 503-518, 2002.
[4] Ambrósio J., Gonçalves J.: Complex Flexible Multibody Systems with Application to Vehicle Dynamics. Multibody System Dynamics, Vol. 6, No. 2, pp. 163-182, 2001.
[5] Kienzle O.: Die Bestimmung von Kräften und Leistungen an spanenden Werkzeugen und Werkzeugmaschinen (in German). Zeitschrift des Vereines Deutscher Ingenieure, Vol. 94, pp. 299-305, 1952.
[6] Paucksch E., Holsten S., LinßM., Tikal F.: Zerspantechnik (in German). Wiesbaden: Vieweg+Teubner, 2008.
[7] Budak E., Altintas Y.: Analytical Prediction of Chatter Stability in Milling – Part I: General Formulation. ASME Journal of Dynamic Systems, Measurement, and Control, Vol. 120, pp. 22-30, 1998.
[8] Henninger C., Eberhard P.: Computation of Stability Bounds for Milling Processes with Parallel Kinematic Machine Tools. Journal of Systems and Control Engineering, Vol. 223, No. 1, pp. 117-129, 2009.
[9] Henninger C., Eberhard P.: Analysis of Dynamic Stability for Milling Processes with Varying Workpiece Dynamics. PAMM Proceedings in Applied Mathematics and Mechanics, Vol. 8, No. 1, pp. 10367-10368, 2008.
[10] Hale J.K., Lunel S.M.V.: Introduction to Functional Differential Equations. New York, Springer, 1993.
[11] Bayly V.B., Davies M.A., Halley J.E., Pratt J.R.: Stability Analysis of Interrupted Cutting with Finite Time in Cut. In Proceedings of the ASME Manufacturing Engineering Division, Vol. 11, pp. 989-996, 2000.
[12] Bayly P.V., Halley J.E., Mann B.P., Davies M.A.: Stability of Interrupted Cutting by Temporal Finite Element Analysis. ASME Journal of Manufacturing Sciences and Engineering, Vol. 125, No. 2, pp. 220-225, 2003.
[13] Insperger T., Stépán G.: Updated Semi-Discretization Method for Periodic Delay-Differential Equations with Discrete Delay. International Journal for Numerical Methods in Engineering, Vol. 61, pp. 117-141, 2004.
[14] Henninger C.: Methoden zur simulationsbasierten Analyse der dynamischen Stabilität von Fräsprozessen (in German). Dissertation, Schriften aus dem Institut für Technische und Numerische Mechanik der Universität Stuttgart, Band 15. Aachen, Shaker Verlag, 2009.
[15] Heisel U., Kang C.: Model-based Form Error Compensation in the Turning of Thin-walled Cylindrical Parts. Production Engineering Research and Development, Vol. 5, No. 2, pp. 151-158, 2010.
[16] Ast A., Eberhard P.: Control Concepts for a Machine Tool with an Adaptronic Actuator. In C. Bottasso; P. Masarati; L. Trainelli (Eds.) Proc. of the ECCOMAS Thematic Conference on Multibody Dynamics, Milano, Italy, 2007.
[17] Ast A., Braun S., Eberhard P., Heisel U.: An Adaptronic Approach to Active Vibration Control of Machine Tools with Parallel Kinematics. Production Engineering Research and Development, Vol. 3, pp. 207-215, 2009.
[18] Preumont A.: Vibration Control of Active Structures. Dordrecht, Kluwer, 2002.
[19] Gawronski W.K.: Advanced Structural Dynamics and Active Control of Structures. New York, Springer, 2004.
[20] Zhou K., Doyle J., Glover K.: Robust and Optimal Control. Upper Saddle River, Prentice Hall, 1996.
[21] Skogestad S., Postlethwaite I.: Multivariable Feedback Control: Analysis and Design. Chichester, John Wiley & Sons, 2nd. Edn., 2005.

Symulacyjna analiza stabilności cienkościennego cylindra podczas toczenia z udoskonaleniem wykorzystującym dłuto tokarskie typu Adaptronic

Streszczenie

Dynamikę procesu toczenia przy obróbce cienkościennego walca zamodelowano stosując teorię giętkich układów wielu ciał. Uzyskano model uwzględniający zmienność w czasie wynikającą z obrotu przedmiotu obrabianego i posuwu narzędzia, a także opóźnienia powodowane wielokrotnym skrawaniem tej samej powierzchni. Niestabilności, które mogą powstać w wyniku tych wielokrotnych skrawań, powinny być wyeliminowane w praktycznych zastosowaniach, gdyż mają one szkodliwe skutki dla przedmiotu obrabianego, narzędzia, a nawet dla maszyny. Pomijając niewielki posuw narzędzia, wynikowa stabilność układu z opóźnieniem i zmiennego w czasie może być analizowana metodą częściowej dyskretyzacji. Badano zastosowanie uchwytu narzędziowego typu Adaptronic, zawierającego siłowniki i czujniki, którego zadaniem jest poprawa stabilności dynamicznej. W symulacji systemu wdrożono różne koncepcje sterowania, dwie kolokacyjne i jedną opartą na modelu, dobierając ustawienia tak, by zwiększyć zakres stabilnego skrawania. W procesie skrawania przedmiotu o umiarkowanie cienkich ścianach występują niestabilności spowodowane głównie wibracjami narzędzia. W tym przypadku granice obszaru stabilności mogą być znacznie poszerzone. Jeśli jednak niestabilność wynika z wibracji przedmiotu obrabianego, koncepcja kolokacyjna zawodzi całkowicie. Koncepcje oparte na modelu mogą nadal zapewniać pewną poprawę, lecz są wrażliwe na błędy modelowania zjawisk na styku przedmiotu obrabianego i narzędzia.